Investigation on the Initial Residual Stress Detection Method and Its Application for Deformation Analysis in Machining Thin-Walled Blades

ZHANG Hua[1], *ZHAO Shengqiang*[1], *SUN Hao*[1], *PENG Fangyu*[1,2], *YAN Rong*[1*], *TANG Xiaowei*[1], *SHAN Yunan*[1]

1. National NC System Engineering Research Center, School of Mechanical Science and Engineering, Huazhong University of Science and Technology, Wuhan 430074, P.R. China; 2. State Key Laboratory of Digital Manufacturing Equipment and Technology, School of Mechanical Science and Engineering, Huazhong University of Science and Technology, Wuhan 430074, P.R. China

(Received 15 July 2023; revised 3 January 2024; accepted 10 April 2024)

Abstract: The thin-walled blade is a crucial component of aero engines, which is highly susceptible to significant deformation during the machining process. Existing research on deformation control focuses on reducing cutting force and machining-induced residual stress (MIRS). The initial residual stress (IRS) generated in the process of heat treatment and forging is used to reduce the deformation of thin-walled parts under the influence of cutting force and MIRS. Because the IRS measurement is difficult and destructive, this paper proposes a reverse identification method of IRS to measure the IRS of Ti6Al4V. The proposed method is more consistent with the trend of stress and deformation distribution compared with the conventional method. To investigate and decouple the interplay between IRS, MIRS and cutting force on machining deformation, this study employs a curved blade for experimental validation and develops a finite element model to predict the deformation. It is found that cutting force accounts for 46.17% of the deformation with an average value of 26.36 μm, while MIRS accounts for 53.83% with an average value of 30.70 μm. Coupling IRS reduces MIRS maximum deflection deformation from 35.32 μm to 15.50 μm, which provides a new approach to optimize machining deformation through IRS distribution.

Key words: thin-walled blade; machining deformation; residual stress analysis; cutting force model

CLC number: V261 **Document code:** A **Article ID:** 1005-1120(2024)02-0158-16

0 Introduction

The thin-walled blade possesses complex profile and strict design tolerance, which has always been regarded as the difficulty in aeronautical manufacturing[1]. Most aviation blades are fabricated from titanium alloy, superalloys or other advanced superalloy materials. To achieve the desired strength of the blanks, most materials are forged, rolled, and heat treated before processing, which introduces the initial residual stress (IRS) inside the blanks and is difficult to measure. The conventional methods for relieving residual stress include thermal stress relief (TSR), vibratory stress relief, and thermal-vibratory stress relief in recent years. And none of these methods can completely eliminate residual stress within the material body[2]. This type of residual stress called as IRS will be released with the removal of materials in the machining process. For aviation thin-walled blades, the machining process typically removes 90% to 95% of blank materials[3]. And this type of part is highly susceptible to IRS release results[4-5], making it crucial to analyze the deformation influence caused by IRS.

*Corresponding author, E-mail address: yanrong@hust.edu.cn.

How to cite this article: ZHANG Hua, ZHAO Shengqiang, SUN Hao, et al. Investigation on the initial residual stress detection method and its application for deformation analysis in machining thin-walled blades[J]. Transactions of Nanjing University of Aeronautics and Astronautics, 2024, 41(2): 158-173.

http://dx.doi.org/10.16356/j.1005-1120.2024.02.003

However, the detection methods of IRS are very complex and destructive. The traditional methods for measuring IRS mainly include the neutron ray method[5], layer removal strain gauge method, layer removal X-ray diffraction method[6], crack compliance method[7], etc. In 2019, Wang et al.[8] enhanced the drilling method by utilizing the strain gauge hole-drilling technique. Employing the inclined plane approach, they boosted the measurement efficiency of IRS by over 50%. Dreier et al.[9] used the theory of layer removal to mill the plate parts, in which the deformation of the remaining workpiece post-layer removal is quantified, and the IRS is determined based on the deformation theory. Gao et al.[10] adopted the crack compliance method to detect IRS in aluminum alloy blank parts, achieving a redistribution of processing allowance for frame parts. Currently, most scholars employ the crack compliance method to measure IRS. However, this approach inevitably results in low measurement efficiency and significant damage to the workpiece.

Therefore, it is necessary to propose a convenient measurement method, which can measure the IRS inside the blank under a small range of failure conditions. Ma et al.[11] proposed that the machining residual stress was seriously affected by the IRS. The initial tensile stress resulted in more extended machining-induced residual stress (MIRS) distribution within the workpiece, whereas the initial compressive stress had the opposite effect. However, the scholar failed to establish a correlation between the residual stress before and after machining. Li et al.[12] also found that the IRS generated in the blank part after heat treatment had an impact on the machining stress of the surface, which made the machining residual stress fluctuate greatly. Zhao et al.[13] discovered the presence of tensile and compressive changes in residual stress induced by machining along the feeding direction and developed a relevant uncertainty model to account for this phenomenon. The reverse identification method is employed in this paper to quantify the IRS in blank materials, which is inherently challenging to measure. The application of reverse identification methods is prevalent in cases where the inputs are challenging to measure, while the outputs can be measured. Zhang et al.[14] established the error mapping between the workpiece features and the corresponding errors in five-axis machining. The source of dynamic and static errors in the workpiece is determined through reverse identification of measurable workpiece features, and error compensation techniques are employed to minimize machining errors. Tian et al.[15] determined the J-C constitutive parameters of inconel 718 alloy under annealing state and precipitated hardened stated with the reverse identification method. By taking the cutting force and chip thickness measured as input, the parameters A, B and n in J-C model are obtained. The reverse identification of IRS can be achieved by analyzing the influence of IRS on machining residual stress.

Once the IRS distribution has been identified, its impact on deformation can be detected through various means. Huang et al.[16] used the finite element method to analyze the deformation relationship between the MIRS and the IRS of the frame parts in the machining process. Indicating that the MIRS accounted for 10% of the deformation, and the IRS accounted for 90% of the deformation. Gao et al.[10] proposed a semi-analytical prediction model for the effect of IRS by using the equivalent bending stiffness, which was combined with the finite element method and mechanical analytical principle. The machining deformation caused by the IRS and tool path in seven typical cases was predicted. Guo et al.[17] proposed a high-precision method for predicting workpiece deformation by amending the IRS slightly based on the support vector machine (SVM) and the genetic algorithm (GA). Aurrekoetxea et al.[18] established a semi-analytical model to study the influence of the IRS on the bending stiffness of a blank. The semi-analytical model mainly considered the volume residual stress in the thickness direction and the MIRS in two directions.

Besides the influence of IRS, thin-walled blades are subject to both cutting force and MIRS factors during the machining process. The MIRS is generated by the cutting process of the tool and is released after the machining, resulting in deflection

deformation. The cutting force is generated by the contact between the tool and the workpiece, which causes the elastic deflection of the blade during the processing, thereby directly causing the processing deformation. Considering the coupling effects of various machining factors is the key for analyzing and predicting the deformation of thin-walled blades.

In terms of MIRS, Yao et al.[19] analyzed the unbalanced distribution of machining residual stress on turbine blades and used the finite element method to predict the overall deformation trend and direction of turbine blades. Masoudi et al.[20] studied the relationship between residual stress and deformation caused by machining on Al7075-T6 aluminum alloy thin-walled cylinder, and the results showed that force and temperature had a direct influence on residual stress and deformation of thin-walled parts. Gulpak et al.[21] proposed a source stress method model for predicting the part shape deviation of 42CrMo4 steel caused by residual stress and material removal changes during processing according to the shape and distribution of the MIRS. In terms of cutting force, Sun et al.[22] proposed a hybrid-driven approach integrating the agent model and Bayesian frame, which focused on the determination error of cutting force during blade machining and comprehensively considered the tool wear and other errors as uncertain errors. Li et al.[23] considered the cutting force error generated by flexible workpieces in five-axis machining, and took the influence of tool run-out into account in the modeling process of cutting force, to better predict the deformation generated by cutting force. Wang et al.[24] proposed a method for predicting static substructure cutting deformation to address the issue of flexible thin-walled workpiece deformation during machining and conducted mirror error compensation to mitigate machining-induced deformation.

It is evident that the cutting force, MIRS, and IRS are crucial factors influencing the machining deformation of thin-walled parts. Analyzing the source of deformation is highly significant, as it enables further control over the influencing factors of machining deformation from its origin.

This paper is structured as shown in Fig.1. Firstly, a reverse identification method (RIM) for

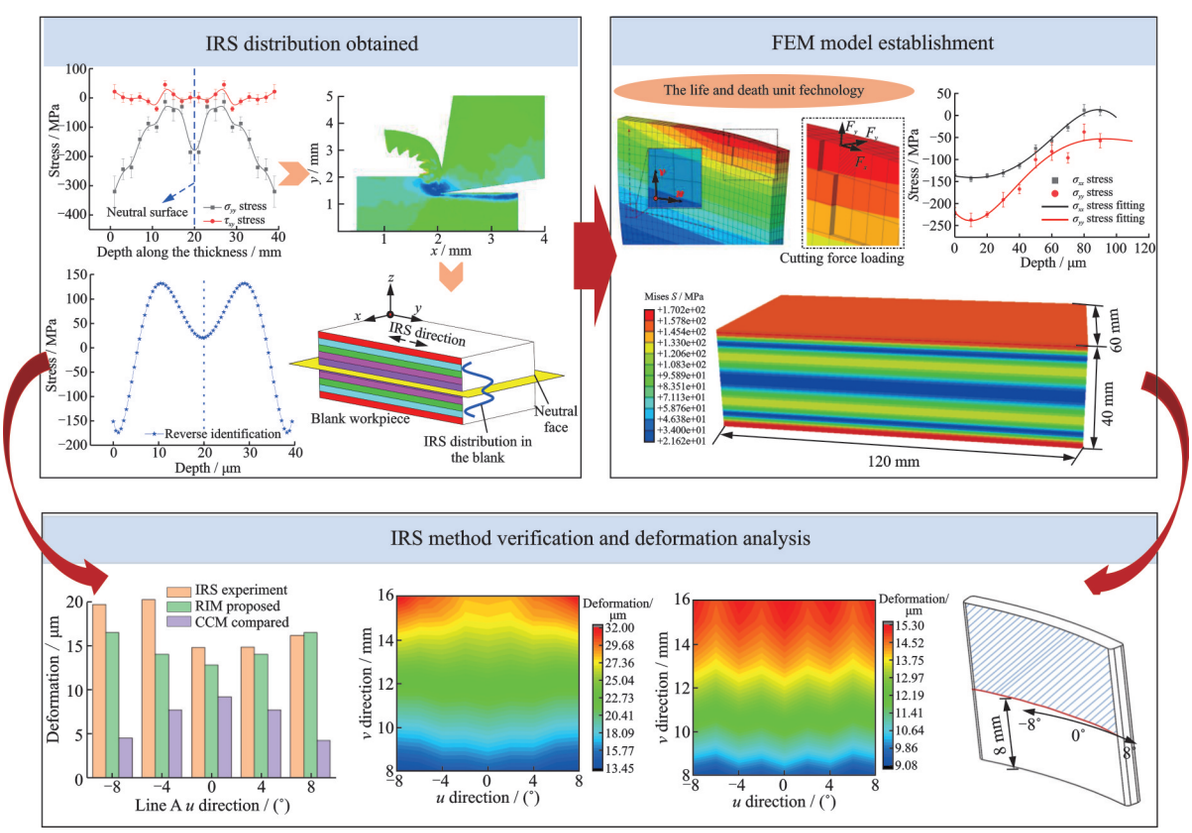

Fig.1 Flowchart of IRS method verification and deformation analysis

IRS measurement is proposed, followed by a comparison using the crack compliance method. Then through the machining process of the blade part, the influence of cutting force, MIRS and IRS is comprehensively considered by establishing the FEM model. Ultimately, the deformation from different sources is analyzed and the IRS distribution for mitigating MIRS deflection deformation is discussed. The CCM stands for the crack compliance method.

1 IRS Detection

As a crucial factor in thin-walled blade processing, the release of IRS seriously affects the machining deformation while the detection methods of IRS are very complex and destructive. In this section, a reverse identification method of IRS based on finite element simulation is proposed to measure the IRS in titanium alloy blank parts. The proposed method has the advantages of less destructive and higher precision. The crack compliance method is utilized for comparison and verification.

1.1 Reverse identification method

The flowchart of the reverse identification method experiment is shown in Fig.2. By analyzing the influence of IRS on MIRS, the reverse identification method was proposed. The reverse identification experiment is conducted on a workpiece made of titanium alloy Ti6Al4V, which is commonly used in critical components such as aero engines due to its high specific strength and excellent high-temperature performance. To investigate the distribution of IRS and blade deformation, the measurement experiment was carried out on the same batch of titanium alloy blank workpieces A, B and C, whose dimensions were 120 mm×40 mm×60 mm. These were respectively used for stress relief heat treatment, reverse identification method and crack compliance method verification. The IRS within the same batch of blank workpieces A, B, and C are assumed to be identical[25].

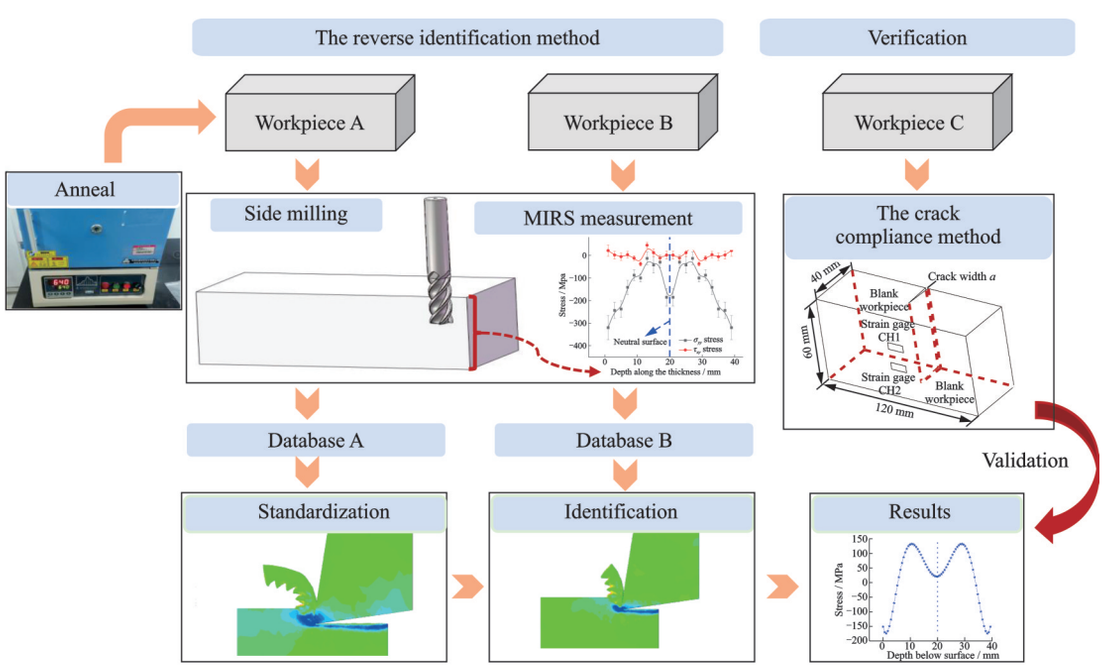

Fig.2 Flowchart of reverse identification method and verification

The blank workpiece A undergoes heat treatment in an annealing furnace, specifically utilizing a KSL1200 box-type resistance furnace for the process. The temperature is initially raised to 600 ℃ at a rate of 100 ℃/h and held for 3 h. After the completion of heat preservation, it is taken out and placed for air cooling.

The wear-resistant tool (CT-JHP780170R04-0.0Z4) is adopted to carry out side milling operations on blank workpieces A and B. Due to the short

side milling distance, the tool wear process in this process is ignored. The chosen parameters for side milling are a_e=0.5 mm, a_p=20 mm, s=1 200 r/min, v=64 m/min and f_z =0.05 mm. The selection of machining parameters is based on two primary criteria: (1) The radial cutting depth is small in milling to avoid excessive influence on the IRS distribution of the workpiece; (2) the processing parameters should be adjusted to target low surface roughness for effective detection (about 20 μm) to meet the test standard of the X-ray analysis system.

The X-ray analysis system produced by Canada Proto company is used to measure the surface MIRS after side milling. Cu is chosen as the target material with a diffraction angle of 142°. The parameters for the X-ray analysis system are presented in Table 1.

Table 1 X-ray analysis system parameter setting

Target	Bragg angle/(°)	$\frac{1}{2}S_1$/Pa^{-1}	$\frac{1}{2}S_2$/Pa^{-1}	Exposure time/s	Voltage/kV	Current/mA
Cu	139.69	11.89	2.83	4	25.0	4.00

The stress amplitude of the workpiece after heat treatment is essentially unchanging along the depth direction. The stress of blank workpiece A after side milling is measured as σ_{yy}=(−198.38±19.07)MPa, τ_{xy}=(−8.2±9.0)MPa.

Fig.3 shows the measured value of MIRS on the surface of blank workpiece B affected by the IRS. It can be observed that the surface distribution is roughly M-shape[26]. The measured MIRS results along the thickness direction are shown in Fig.3 and Table 2. Due to the processing characteristics of forging and heat treatment processes[27], it is considered that the IRS is distributed symmetrically along the neutral surface.

As a bridge between practice and theory, the FEM is used to establish the relationship between IRS and MIRS. Third Wave AdvantEdge is a commercial software that provides guidance for machining simulation. The IRS loading function of the software is used to build the finite element simulation

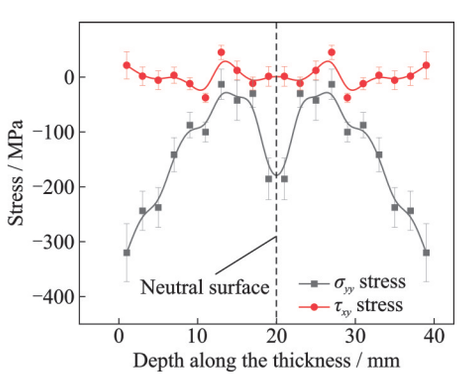

Fig.3 MIRS results of workpiece B after side milling

Table 2 MIRS results of workpiece B in detail

Depth/mm	σ_{yy}/MPa	τ_{xy}/MPa
2	−320.8	21.4
4	−243.68	1.7
6	−237.63	−5.8
8	−141.46	3.2
10	−87.49	−12.1
12	−100.21	−37.8
14	−13.21	−45.1
16	−42.33	−12.0
18	−30.15	11.6
20	−185.6	−1.3

verification database and the reverse calculation database, so as to identify the IRS in reverse.

The experiment needs that the IRS inside workpiece A be marked as zero. In the simulation process of the blank workpiece, simplified parameters are utilized. The purpose of a simplified setting is to reduce the finite element simulation time and obtain more stable simulation data. The overall length involved in the cutting process is simplified in order to reduce the simulation time, and a subset of stable cutting data comprising 30%—60% of the cutting path is extracted as the target data at approximately 1 mm which is utilized for simulating the cutting process in a single-tooth milling state. In the process of finite element simulation, orthogonal turning is used to replace the milling simulation process due to the significantly large ratio of tool diameter to cutting width in the machining parameters. Ac-

cording to the conversion of milling and turning, some optimization and setting of simulation parameters are needed. And the effective average rake angle α_e is used to replace the rake angle for simulation which is displayed as[28]

$$\alpha_e = \arctan\left[-\frac{\sqrt{\left(2-\varsigma h_a/r_e\right)\varsigma h_a/r_e}-\sin\theta_f}{\varsigma h_a/r_e-1+\cos\theta_f}\right] \tag{1}$$

where h_a is the cutting thickness; r_e the cutting tool edge radius of the circular arc; ς the empirical constant number, which is calculated as 2; and θ_f the separation angle of the cutting tool and chip separation, which is calculated as 37.6°. The specific representation of parameters is shown in Fig.4.

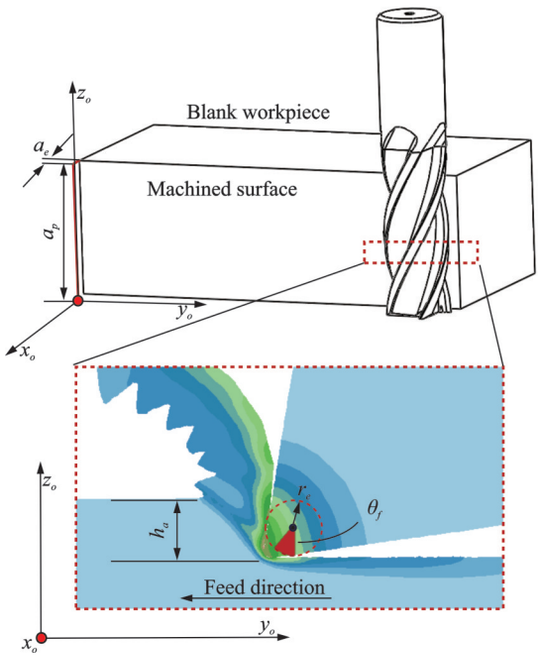

Fig.4 Schematics for side milling in detail

Fig.5 shows the finite element simulation results loaded with different initial residual stresses. Different groups of IRS are loaded in the finite element simulation, and 20 MPa is taken as a stress gradient. Ten groups of initial data are simulated from −160 MPa to 20 MPa, providing a database for reverse identification.

After establishing the database of IRS and MIRS, the reverse identification theory requires an analysis of the mapping relationship between them. The neural network structure in MATLAB is employed for fitting purpose. The concept of reverse identification stems from establishing a mapping relationship between inputs that are challenging to measure and outputs that can be measured. As shown in Fig.6, the mapping relationship between the IRS and MIRS is established by utilizing a finite element simulation database. This mapping relationship is fitted to a multi-layer neural network. Subsequently, the input of experimental surface MIRS enables the determination of the difficult-to-measure IRS.

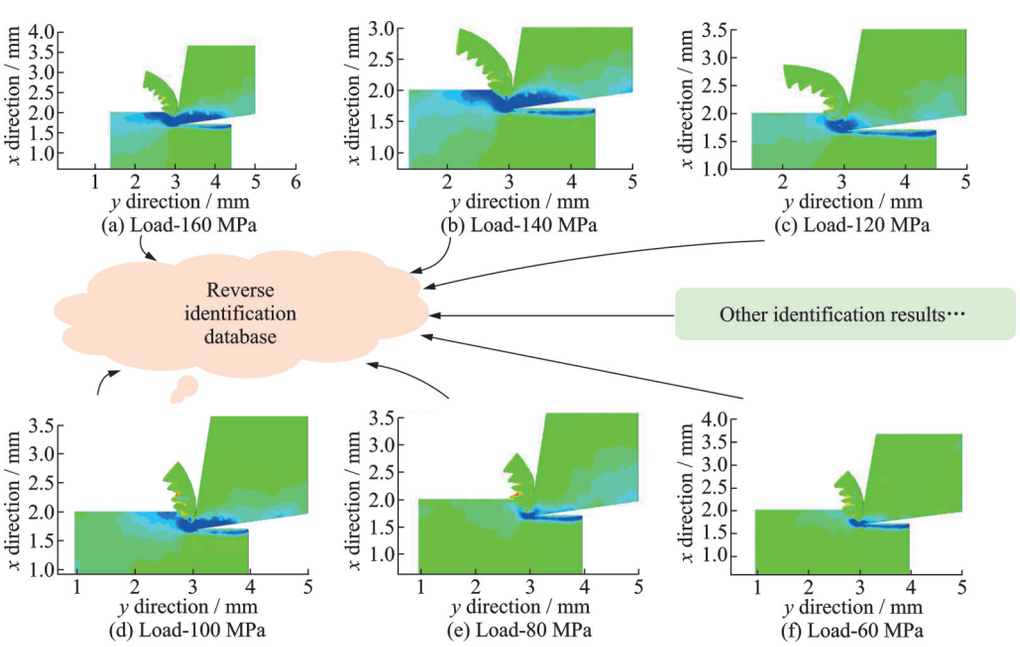

Fig.5 Establishment of the database for RIM

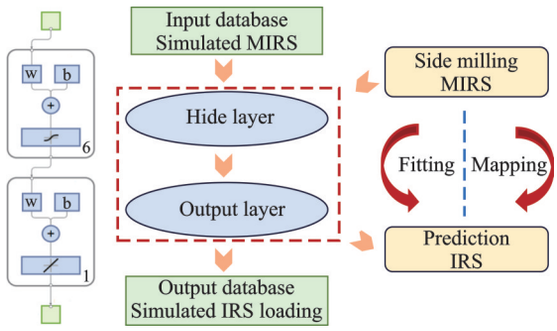

Fig.6 Construction of the reverse identification model

Due to the heat treatment and forging process of the blank before machining, the IRS distribution is approximately considered to be uniform along each layer[25]. The concept of reverse identification has been employed to determine the IRS of the blank by analyzing the MIRS states on the surface of workpiece B. The specific results obtained through RIM are presented in Fig.7.

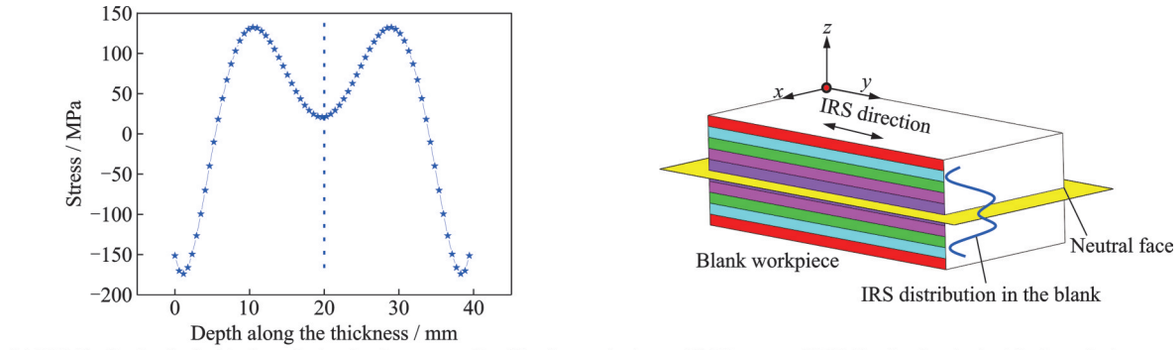

(a) IRS distribution in the blank workpiece by the reverse identification method (b) Diagram of IRS distribution in the blank workpiece

Fig.7 IRS distribution in the blank workpiece by the reverse identification method and its diagram

1.2 Comparison and analysis of method

To validate the accuracy of the reverse identification method, the crack compliance method is employed to confirm the results. The crack compliance method is a longitudinal cutting technique used to measure the IRS. At present, many scholars used the crack compliance method to measure IRS[29]. The principle is shown in Fig.8. A crack is introduced by wire electrical discharge machining (WEDM). The IRS is released by progressively cutting the material at increasing depth.

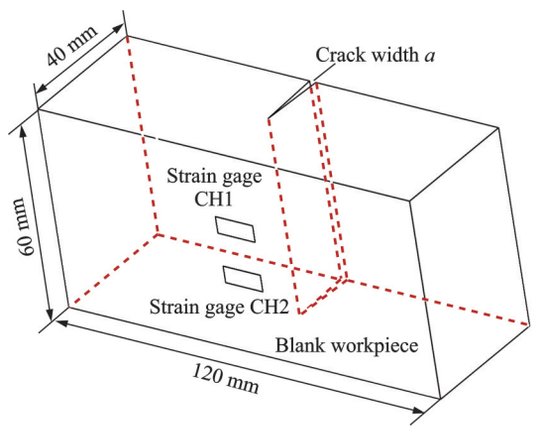

Fig.8 Diagram of the crack compliance method

The crack compliance method is used to obtain the IRS along the depth direction of the blank workpiece. The blank workpiece satisfies the force and moment equilibrium conditions under the loading of the Legendre polynomial. Measurement of the release strain and slit depth enables subsequent calculation of the stress distribution $\sigma_{yy}(x)$ as shown in

$$\sigma_{yy}(x)=\sum_{j=2}^{m}A_jP_j(x) \tag{2}$$

$$\boldsymbol{A}=\left[(\boldsymbol{C}^{\mathrm{T}}\boldsymbol{C})^{-1}\boldsymbol{C}^{\mathrm{T}}\right]\varepsilon_{\mathrm{ave}} \tag{3}$$

$$C_{ij}=\varepsilon(a_i)\big|_{\sigma=P_j(x)} \tag{4}$$

where $\boldsymbol{A}$ is the undetermined coefficient matrix and the calculation method of matrix $\boldsymbol{A}$ is shown in Eq.(3) and $P_j(x)$ the Legendre polynomials. m represents the order of the Legendre function, which is determined to be 7[24]; $\boldsymbol{C}$ is referred to the flexibility matrix, which is the strain matrix produced by the influence of the Legendre function on the blank workpiece. i indicates the number of crack propagation and $\varepsilon_{\mathrm{ave}}$ the experimental average strain value of CH1 and CH2. The calculation of the flexibility matrix is represented in Eq.(4).

The loading of the Legendre function is shown in Fig.9(a). The strain generated by the crack is shown in Fig.9(b). Based on the strain results obtained from the Legendre polynomial in FEM and substituted into Eq.(2), the IRS is determined, as illustrated in Fig.10.

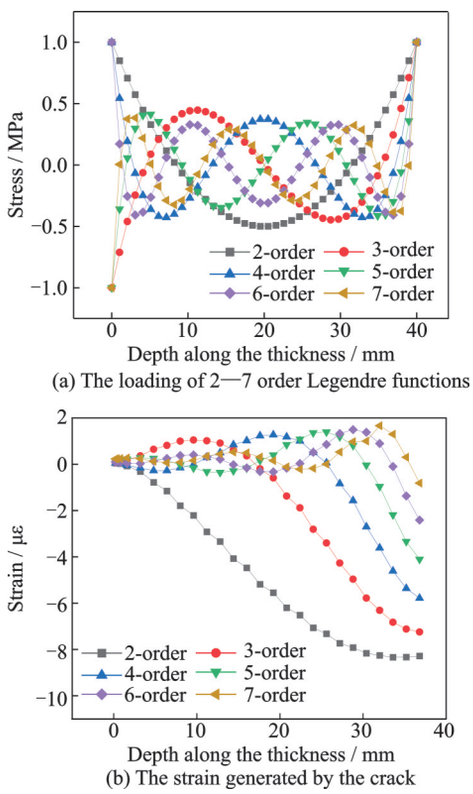

Fig.9 The crack compliance method for IRS measurement

By analyzing and comparing the distribution of the measurement results of the two methods, the accuracy of the proposed method is evaluated in terms of the forging and heat treatment processes applied to the blank workpiece, as shown in Fig.11.

The IRS after the reverse identification method

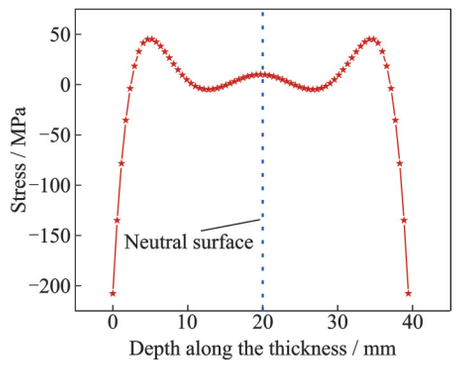

Fig.10 IRS distribution of workpiece C by the crack compliance method

presents the situation of pressing and stretching in the whole blank, and the overall shape is an M-shape. The minimum stress on the neutral surface is approximately −20 MPa, while the maximum compressive stress is distributed symmetrically across both sides of the blank workpiece. Additionally, the maximum tensile stress is concentrated in 1/4 of the blank. The statement conforms to the legal distribution of forged workpieces. In terms of the crack compliance method, the maximum value of the IRS is distributed at both ends of the blank, which is about −180 MPa, and then rises slowly. The IRS fluctuates from about 30 MPa to 0 MPa around the neutral face, showing an overall M distribution. The closer to the neutral surface, the gentler the change of the stress.

The reverse identification method proposed in this paper is consistent with the normal stress size, trend and shape of crack compliance. The reverse identification method provides a more accurate reflection of the residual stress distribution within the workpiece, as evidenced by the deformation observed in section 3.1. As for the crack compliance

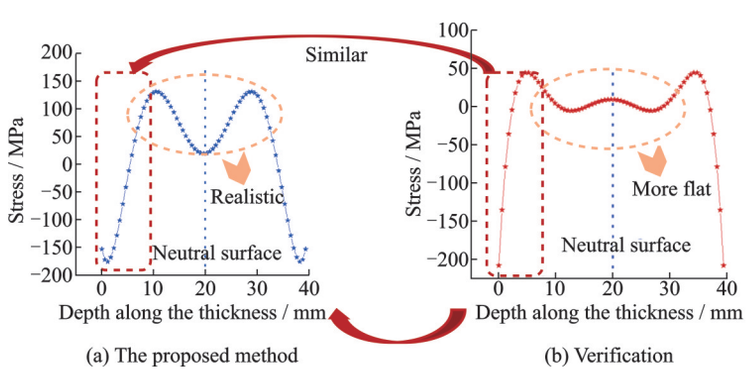

Fig.11 Comparison results between the proposed method and verification

method, it is smoother near the neutral surface due to the fitting of the high-order Legendre function.

2 Deformation Prediction Model and Experiment

After obtaining the distribution of IRS, a FEM model considering IRS, MIRS and cutting force is established to analyze the different influence of these three factors, as shown in Fig.12. The cutting force is the main deformation source in the thin-walled blade machining process. The release of IRS and MIRS will lead to the deflection deformation[20,30]. Using the IRS obtained by the reverse identification method of the IRS of titanium alloy in Section 1, a blade is used for machining experiments and deformation measurement. The feature of the blade in this experiment is selected from the actual ruled surface blade. The influence of muti-factors on the deformation in the machining process is discussed in coupling.

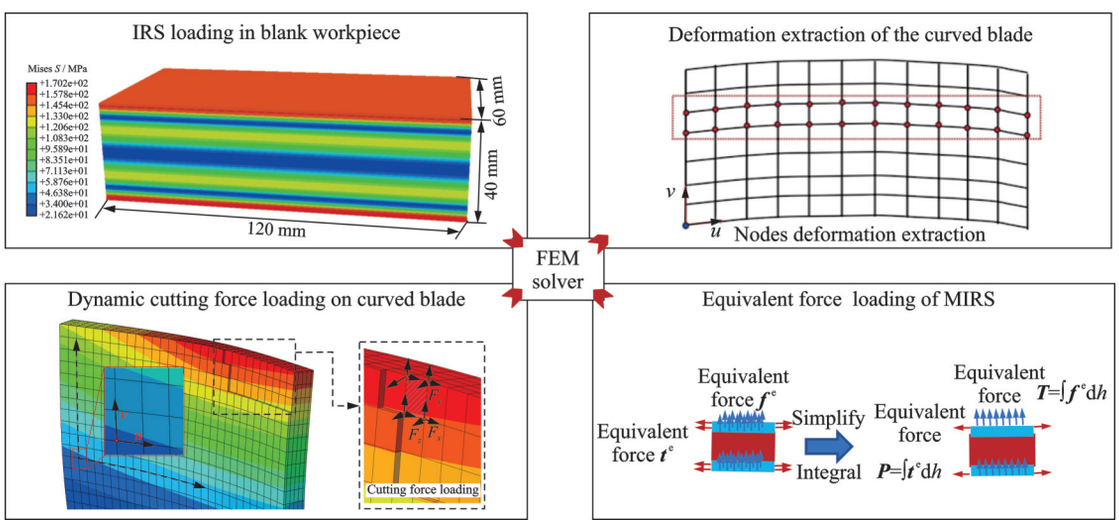

Fig.12 The FEM model for the curved blade deformation prediction and analysis

2.1 Establishment of thin-walled blade FEM model

2.1.1 IRS distribution loading

As a kind of stress released, IRS is rarely considered in the machining process when blank material is removed. When the distribution of the blank residual stress is known, the finite element method can be used to study the impact of IRS on machining deformation. The specific finite element settings are shown as follows.

The loading of the IRS field is realized based on the SIGINI subroutine as shown in Fig.13. In the deformation analysis of the curved blade, the IRS along the deflection direction (σ_{yy}) is the main source of deformation, which is loaded by the SIGINI subroutine in FEM. The size of the blank is set as 120 mm×60 mm×40 mm and the simulation accuracy of each layer is set as 0.5 mm. The IRS (σ_{yy}) obtained by the crack compliance method and reverse identification method can be selected from Section 1.

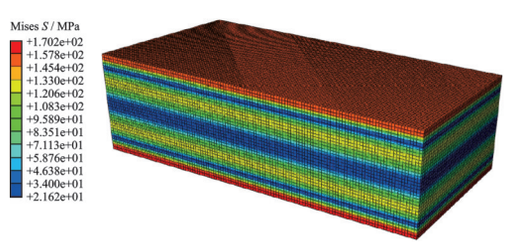

Fig.13 IRS loading based on SIGINI subroutine

2.1.2 Dynamic cutting force loading

Dynamic loading of cutting force and material removal is carried out by ABAQUS software. As shown in Fig.14, to simulate the removal of workpiece materials and dynamic loading of cutting force in the actual processing, the life and death unit technology is adopted. This technology is to multiply the material attribute of the matrix element by a very small coefficient so that the element is killed

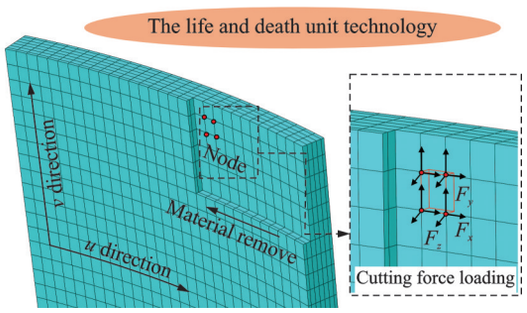

Fig.14 The life and death unit technology and dynamic loading of cutting force

and the influence on other elements is eliminated.

The dynamic loading of cutting force is carried out by Python development. The changing of cutting force over time is dynamically loaded to grid nodes, which achieve the fitting of the simulation process and the actual process. The Johnson-Cook constitutive material attribute of Ti6Al4V[31] was attributed to the entire workpiece material, and the meshes were partitioned using the C3D8R mesh type. Ultimately, a total of 6 167 meshes were generated.

2.1.3 MIRS equivalence loading

The impact of MIRS on deformation cannot be disregarded, with an influence depth ranging from 100—200 μm. Due to the complexity of the curved surface, the deformation influence of MIRS is analyzed and the deformation prediction model of the blade workpiece is established based on the source stress method[21].

In the application of the source stress method, the effect of MIRS can be equivalent to shear loading and face loading. The calculation[19] of the equivalent shear force $\boldsymbol{T}$ and face force $\boldsymbol{P}$ are shown in Eqs.(5—8). With the loading of equivalent shear force and face force in FEM, the deformation influence of MIRS can be analyzed.

$$\boldsymbol{T}=\int_0^{H_0}\boldsymbol{f}^{\mathrm{e}}\mathrm{d}h \tag{5}$$

$$\boldsymbol{P}=\int_0^{H_0}\boldsymbol{t}^{\mathrm{e}}\mathrm{d}h \tag{6}$$

$$\boldsymbol{f}^{\mathrm{e}}=-\nabla\boldsymbol{\sigma}^{\mathrm{mech}} \tag{7}$$

$$\boldsymbol{t}^{\mathrm{e}}=\boldsymbol{\sigma}^{\mathrm{mech}}\cdot\boldsymbol{n} \tag{8}$$

where H_0 is the MIRS influence depth; $\mathrm{d}h$ the differential of MIRS influence depth; $\boldsymbol{\sigma}^{\mathrm{mech}}$ the MIRS tensor; and $\boldsymbol{n}$ the normal vector along the feed direction, as shown in Fig.15.

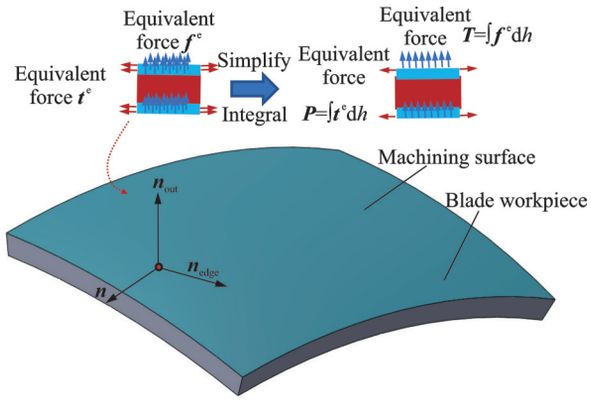

Fig.15 The loading and simplifying of MIRS by source stress method

2.2 Thin-walled blade experiment setup

In the experimental process, the SECO milling tool (553080Z3.0-SIRON-A) is utilized for rough and semi-finishing machining, and the SHANHELE wear-resistant milling tool (SHANHELE-8×8D×4T×60L) is employed for finishing machining. The machining experiments are conducted exclusively on the Mikron UCP800, a five-axis machining center. The processing parameters and material parameters are shown in Table 3 and Table 4[32]. Regenerative chatter resulting from dynamic cutting forces can lead to uneven surface stress states[33-34], which are evidenced by residual stress fluctuations along the machining direction[35]. To mitigate the non-uniform effects of regenerative chatter on MIRS, smaller cutting parameters and slower feed speeds are employed during the finishing processes.

The NI acquisition system and the three-coordinate system are utilized to measure the cutting force generated during the machining process. As shown in Fig.16, the cutting force measurement system is composed of a display, charge amplifier and NI acquisition. The Kistler9124B dynamic dynamometer is used to measure the cutting force.

Table 3 Machining parameter setting

Processing method	f_z/(mm•r^{-1})	v/(m•s^{-1})	a_p/mm	a_e/mm
Rough	0.04	60	1	—
Semi-finish	0.03	60	3	0.5
Finish	0.02	66	3	0.2

Table 4 Ti6Al4V physical properties[32]

Density/ ($kg \cdot m^{-3}$)	Poisson's ratio	Elasticity/ GPa	Thermal conductivity/ ($J \cdot kg^{-1} \cdot ℃^{-1}$)	Conductivity/ ($W \cdot m^{-1} \cdot ℃^{-1}$)	Young's modulus/ MPa
4 430	0.34	104.5	7.4	624	894.903

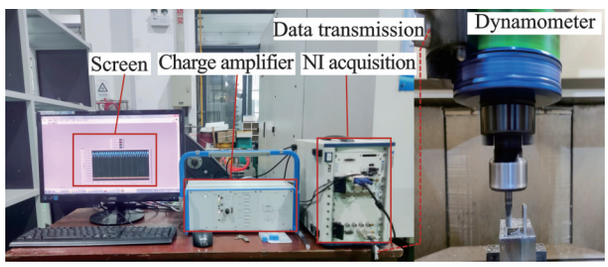

Fig.16 Machining process and measurement of cutting force

The three-coordinate system is utilized to detect the machining deformation of the blade workpiece with a maximum allowable error detection of 1.7 μm. The schematic diagram of the measured points and their distribution positions are shown in Figs.17 and 18. The primary blade deformation occurs in the deflection direction caused by the y-directional IRS. It is widely believed that IRS is distributed in layers[25].

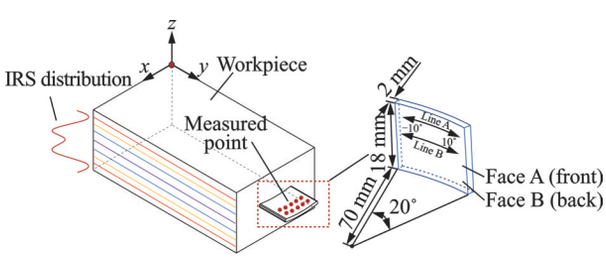

Fig.17 Stress distribution and measurement position

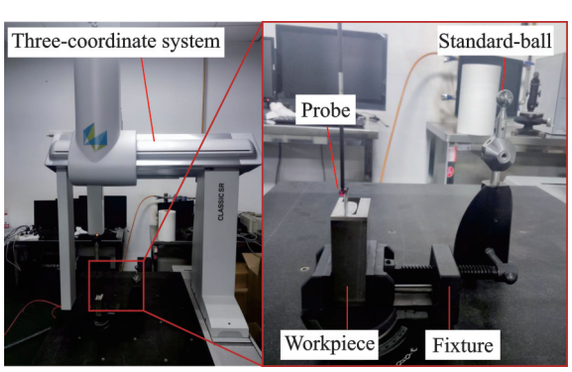

Fig.18 Blade deformation measurement in the three-coordinate system

The MIRS below the surface of 200 μm is measured so as to integrate or differentiate the shear force and face force in the actual simulation loading process. And the MIRS experiment setup is shown in Fig.19.

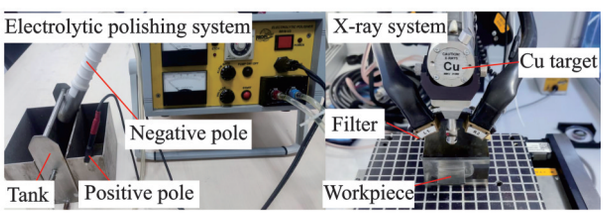

Fig.19 Electrolytic polishing experiment and MIRS measurement experiment

Using the electrolytic polishing system, the MIRS of the front blade and back blade of the workpiece are respectively measured. The radius of the negative pole is 5 mm, the polishing voltage is 30 V, the polishing velocity is 2.5 cm^3/s, and the polishing current is 2 A. It comes to that the speed of polishing is 10 μm/s. The measurement results of MIRS are shown in Fig.20.

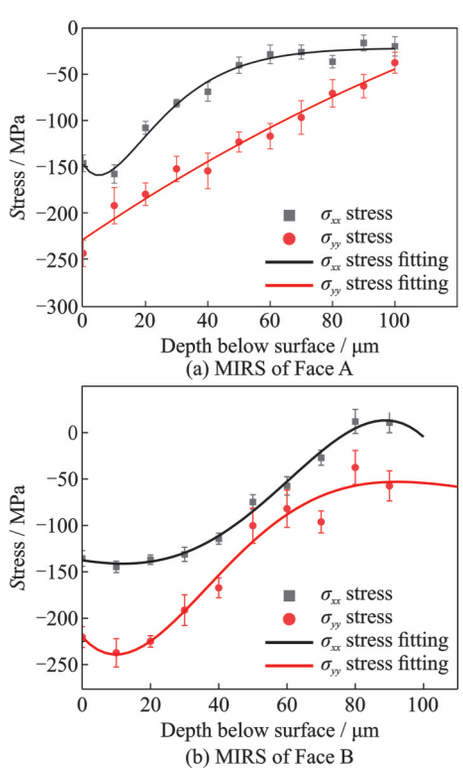

Fig.20 MIRS distribution in the x and y directions(x represents the feed direction and y the vertical feed direction)

3 Results and Discussion

3.1 Deformation verification of the reverse identification method

In order to intuitively compare the precision difference between the reverse identification method and the crack compliance method, the IRS obtained in Section 1 is taken as the input of the finite element solver to observe the deformation output. By comparing the deflection deformation of the blade workpiece subjected to IRS, the experimental results are shown in Fig.21.

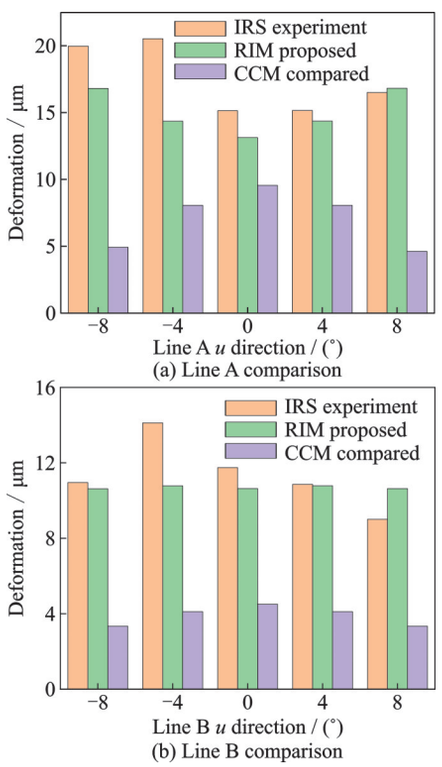

Fig.21 Comparison of different IRS measurement method simulation deformation and experiment deformation

The results indicate that the deformation caused by RIM is consistent with the influence of actual IRS on the blade, whereas the deformation acquired through the crack compliance method differs significantly. The crack compliance method is highly effective in detecting the IRS at the edge of the blank. And the method is affected by the high-order Legendre function, which causes smooth stress fluctuation near the neutral surface. The RIM can reflect the real tension and pressure state close to the neutral surface.

3.2 Multi-factors-induced deformation analysis

The deformation results caused by cutting force are shown in Fig.22. The deformation at the 17 mm height (Line A in Fig.17) and 14 mm height (Line B in Fig.17) of the blade are measured with the three-coordinate system, respectively. Deformation results of the MIRS and cutting force are obtained in the finite element method, as shown in Fig.22. The maximum deformation occurs at the blade edge, which is primarily influenced by cutting in and cutting out.

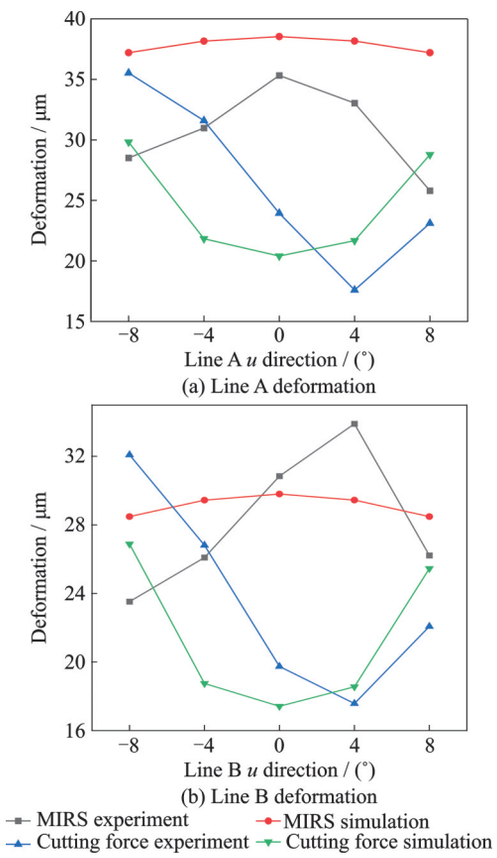

Fig.22 Deformation caused by MIRS and cutting force in simulation and experiment

During the process of experimentation and simulation, the MIRS at the 0° position is utilized to represent the MIRS of the entire curved blade. However, due to dynamic cutting forces, the MIRS at other positions exhibit fluctuations, resulting in disparities between simulated and experimental deformation. Nevertheless, there exists a discernible trend where deformation initially increases and subsequently decreases. The error measured precisely at 0° position between experiment and simulation is

within 5 μm.

Due to the inherent coupling relationship between MIRS and IRS, the curved blade machining process was carried out on workpiece B where the IRS and MIRS had been measured. The selection of the blade distribution position will lead to increased or decreased deflection deformation[25]. The distribution position of the blade in the machining process is shown in Fig.23. It is located in the area where the influence of IRS is negative to the deflection deformation caused by the MIRS. The simulation and experiment results of workpiece B for Line A and Line B are obtained, as shown in Fig.24.

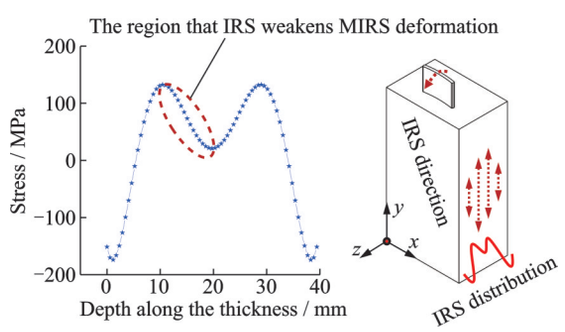

Fig.23 Selection of blade distribution position in the blank workpiece

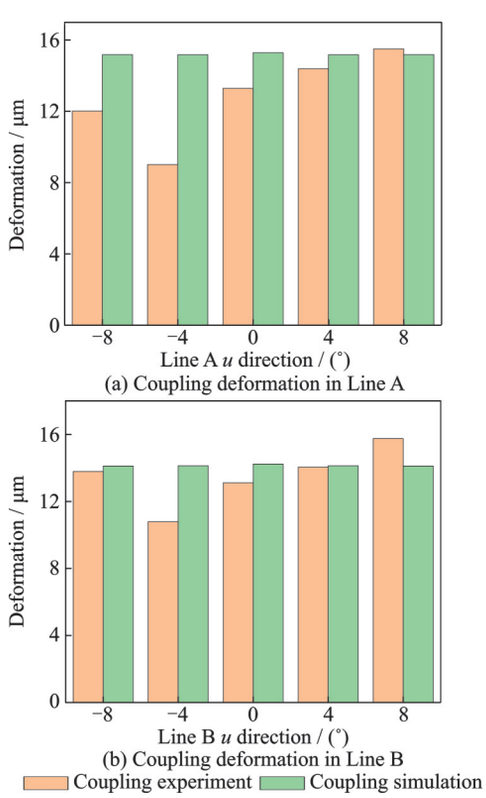

Fig.24 Simulation and experiment of coupling IRS with MIRS

And the simulation results caused by MIRS are shown in Fig.25. The maximum deformation is at the upper end of the blade and near the edge of the blade, which is about 32 μm. The deformation in the middle of the blade is relatively gentle, about 22 μm. As for the simulation results coupling of MIRS and IRS shown in Fig.26, the overall deformation decreases. The maximum deformation value appears at the upper end of the blade, which is about 15 μm.

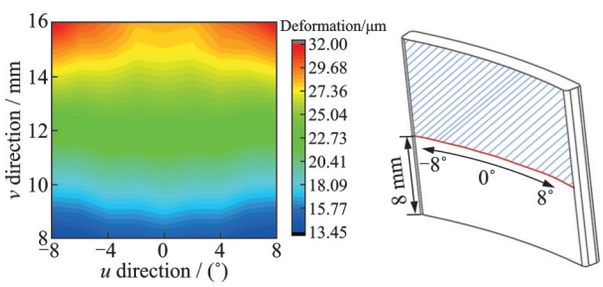

Fig.25 FEM simulation deformation distribution of MIRS

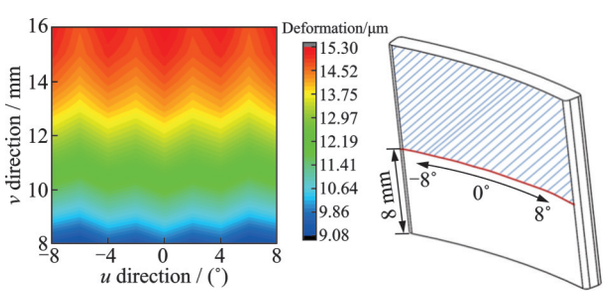

Fig.26 FEM simulation deformation distribution of coupling MIRS and IRS

Coupling the influence of cutting force and MIRS, as shown in Fig.22, the maximum deformation caused by the cutting force is 35.50 μm which appears on the edge of the blade affected by tool cutting in and out. The mean value of deformation caused by MIRS in Line A is 30.73 μm accounting for 53.83%, while the cutting force contributes to 46.17% of the influence with a mean value of 26.36 μm. The MIRS has a significant influence on the thin-walled blade deformation contrast with the cutting force. It shares the same phenomenon at different heights of the blade (Line A and Line B). However, the blade maximum deflection deformation caused by MIRS is decreased by using the distribution of the IRS, as shown in Fig.23. The maxi-

mum deflection deformation comes to 15.50 μm, which decreases 56.12% than only considering the MIRS, as shown in Fig.22 and Fig.24. The special distribution location IRS has a negativity effect on the deflection deformation caused by MIRS. The maximum deflection deformation decreases from 35.32 μm to 15.50 μm.

4 Conclusions

The initial proposed application for the reverse identification method (called RIM in this paper) between IRS and MIRS is made. The crack compliance method is employed for the verification of the RIM, which obtains the effectiveness and rationality of the proposed method. The influence of the IRS is considered to reduce the deflection deformation caused by MIRS. The coupling deformation effect of cutting force, MIRS and IRS on the curved blade are analyzed and the following conclusions can be drawn:

(1) The innovative reverse identification method of IRS measurement is proposed. Compared with the crack compliance method, it can measure the IRS inside the blank workpiece with higher accuracy near the neutral surface, which is verified through the deformation analysis caused by IRS. The IRS inside the blank material shows the state of external tension and internal compression.

(2) By coupling cutting force and MIRS in the machining process, it is found that cutting force deformation accounts for 46.17% of the total influence with a mean value of 26.36 μm, while MIRS contributes to 53.83% of the influence with a mean value of 30.73 μm. Coupling and considering the special location of the IRS, the total deflection deformation decreases to an average of 14.67 μm. The maximum deflection deformation is reduced by 56.21%. The deformation proportion resulting from IRS, cutting, and MIRS is analyzed through finite element simulation and experiment, providing valuable insights for future optimization of machining deformation.

(3) In the machining process of the thin-walled blade, the release of MIRS after machining is considered, which will cause deflection deformation of the blade. The IRS inside the blank materials is released after material removal, which will also cause deflection deformation of the blade. While considering the distribution position of IRS in the blank, the deflection deformation caused by MIRS is weakened. The concept of superposition cancellation is employed to mitigate machining deformation caused by multiple factors.

In the future, from the perspective of the source of deformation, controlling the cutting force will improve the machining accuracy more quickly. The influence of MIRS can be weakened by machining parameters to reduce deformation. In terms of IRS, most of the current methods are stress relief annealing to avoid the influence of the factor. However, after knowing the distribution of IRS, it can be introduced into the machining system as a deformation resistance factor, which will provide a new solution for the control of machining deformation.

References

[1] ZHANG Yun, ZHU Yu, ZHU Zhengqing. An error area determination approach in machining of aero-engine blade[J]. Transactions of Nanjing University of Aeronautics and Astronautics, 2022, 39(3): 349-357.

[2] GAO H, LI X, LI B, et al. Residual stress and microstructure of Ti6Al4V treated by thermal-vibratory stress relief process[J]. Journal of Materials Research and Technology, 2022, 18: 5161-5181.

[3] CHANTZIS D, VAN-DER-VEEN S, ZETTLER J, et al. An industrial workflow to minimise part distortion for machining of large monolithic components in aerospace industry[J]. Procedia CIRP, 2013, 8: 281-286.

[4] CASUSO M, POLVOROSA R, VEIGA F, et al. Residual stress and distortion modeling on aeronautical aluminum alloy parts for machining sequence optimization[J]. The International Journal of Advanced Manufacturing Technology, 2020, 110: 1219-1232.

[5] LEVIEIL B, BRIDIER F, DOUDARD C, et al. Experimental comparison of in-depth residual stresses measured with neutron and X-ray diffraction with a numerical stress relaxation correction method[J]. Materials Science Forum, 2017, 905: 131-136.

[6] GUO J, FU H, PAN B, et al. Recent progress of residual stress measurement methods: A review[J]. Chinese Journal of Aeronautics, 2021, 34: 54-78.

[7] AKHTAR W, LAZOGLU I, LIANG S Y. Prediction and control of residual stress-based distortions in the machining of aerospace parts: A review[J]. Journal of Manufacturing Processes, 2022, 76: 106-122.

[8] WANG Z, SUN J, LIU L, et al. An analytical model to predict the machining deformation of frame parts caused by residual stress[J]. Journal of Materials Processing Technology, 2019, 274: 116282.

[9] DREIER S, DENKENA B. Determination of residual stresses in plate material by layer removal with machine-integrated measurement[J]. Procedia CIRP, 2014, 24: 103-107.

[10] GAO H, ZHANG Y, WU Q, et al. Investigation on influences of initial residual stress on thin-walled part machining deformation based on a semi-analytical model[J]. Journal of Materials Processing Technology, 2018, 262: 437-448.

[11] MA Y, YU D, FENG P, et al. Finite element method study on the influence of initial stress on machining process[J]. Advances in Mechanical Engineering, 2015. DOI:10.1177/1687814015572457.

[12] LI B, JIANG X, YANG J, et al. Effects of depth of cut on the redistribution of residual stress and distortion during the milling of thin-walled part[J]. Journal of Materials Processing Technology, 2015, 216: 223-233.

[13] ZHAO S, SUN H, PENG F, et al. Parametric characterization and distribution consistency evaluation of machining-induced residual stress[J]. Journal of Manufacturing Science and Engineering, 2022, 145: 1-29.

[14] ZHANG H, XIANG S, LIU C, et al. Reverse identification of dynamic and static motion errors for five-axis machine based on specimen feature decomposition[J]. ISA Transactions, 2023, 134: 302-311.

[15] TIAN P, HE L, ZHOU T, et al. Reverse identification of constitutive parameters of inconel 718 alloy based on analytical model and thermo-mechanical loads analysis of machined surface[J]. Journal of Materials Research and Technology, 2022, 16: 1353-1370.

[16] HUANG X, SUN J, LI J. Finite element simulation and experimental investigation on the residual stress-related monolithic component deformation[J]. The International Journal of Advanced Manufacturing Technology, 2014, 77: 1035-1041.

[17] GUO J, WANG B, HE Z X, et al. A novel method for workpiece deformation prediction by amending initial residual stress based on SVR-GA[J]. Advances in Manufacturing, 2021, 9: 483-495.

[18] AURREKOETXEA M, LLANOS I, ZELAIETA O, et al. Improving accuracy of bulk residual stress characterization in ribbed geometries through equivalent bending stiffness[J]. Procedia CIRP, 2021, 102: 325-330.

[19] YAO C, ZHANG J, CUI M, et al. Machining deformation prediction of large fan blades based on loading uneven residual stress[J]. The International Journal of Advanced Manufacturing Technology, 2020, 107: 4345-4356.

[20] MASOUDI S, AMINI S, SAEIDI E, et al. Effect of machining-induced residual stress on the distortion of thin-walled parts[J]. The International Journal of Advanced Manufacturing Technology, 2015, 76: 597-608.

[21] GULPAK M, SÖLTER J, BRINKSMEIER E. Prediction of shape deviations in face milling of steel[J]. Procedia CIRP, 2013, 8: 15-20.

[22] SUN H, PENG F, ZHOU L, et al. A hybrid driven approach to integrate surrogate model and Bayesian framework for the prediction of machining errors of thin-walled parts[J]. International Journal of Mechanical Sciences, 2021, 192: 106111.

[23] LI Z L, TUYSUZ O, ZHU L M, et al. Surface form error prediction in five-axis flank milling of thin-walled parts[J]. International Journal of Machine Tools and Manufacture, 2018, 128: 21-32.

[24] LI W, WANG L, YU G. Force-induced deformation prediction and flexible error compensation strategy in flank milling of thin-walled parts[J]. Journal of Materials Processing Technology, 2021, 297: 117258.

[25] YANG Y, LI X, LI L, et al. Investigation on deformation of single-sided stringer parts based on fluctuant initial residual stress[J]. Journal of Materials Processing Technology, 2019, 271: 623-633.

[26] LI X, LI L, YANG Y, et al. Machining deformation of single-sided component based on finishing allowance optimization[J]. Chinese Journal of Aeronautics, 2020, 33: 2434-2444.

[27] KE Yinglin, DONG Huiyue. Pre-stretching process and its application in reducing residual stress of quenched 7075 aluminum alloy thick-plates[J]. The Chinese Journal of Nonferrous Metals, 2004(4): 639-645. (in Chinese)

[28] ZENG H H, YAN R, PENG F Y, et al. An investigation of residual stresses in micro-end-milling considering sequential cuts effect[J]. The International Journal of Advanced Manufacturing Technology, 2017, 91: 3619-3634.

[29] PRIME M B, HILL M R. Residual stress, stress relief, and inhomogeneity in aluminum plate[J]. Scripta Materialia, 2002, 46: 77-82.

[30] GAO H, LI X, WU Q, et al. Effects of residual

stress and equivalent bending stiffness on the dimensional stability of the thin-walled parts[J]. The International Journal of Advanced Manufacturing Technology, 2022, 119: 4907-4924.
[31] XU B, ZHANG J, LIU X, et al. Fully coupled thermomechanical simulation of laser-assisted machining Ti6Al4V reveals the mechanism of morphological evolution during serrated chip formation[J]. Journal of Materials Processing Technology, 2023, 315: 117925.
[32] JOHNSON G R, COOK W H. Fracture characteristics of three metals subjected to various strains, strain rates, temperatures and pressures[J]. Engineering Fracture Mechanics, 1985, 21: 31-48.
[33] CHENG Kai. Machining dynamics: Fundamentals, applications and practices[M]. [S.l.]: Springer, 2009.
[34] WANG P, BAI Q, CHENG K, et al. Investigation on an in-process chatter detection strategy for micro-milling titanium alloy thin-walled parts and its implementation perspectives[J]. Mechanical Systems and Signal Processing, 2023, 183: 109617.
[35] ZHAO S, PENG F, SUN H, et al. Physical multi-factor driven nonlinear superposition for machining deformation reconstruction[J]. International Journal of Mechanical Sciences, 2023, 262: 108723.

Acknowledgments This work was financially supported in part by the National Key Research and Development Program of China (No.2022YFB3404803) and the National Natural Science Foundation of China (No.92160301).

Authors Mr. **ZHANG Hua** received the B.S. degree in mechanical engineering from Huazhong University of Science and Technology, Wuhan, China, in 2021 and is pursuing the M.S. degree with Huazhong University of Science and Technology. His research interest includes thin-walled parts deformation analysis for aviation and residual stress deformation.

Prof. **YAN Rong** received her Ph.D. degree in mechanical engineering from Wuhan University, Wuhan, China, in 2005. From 2005 to 2007, she worked as a postdoctoral fellow at Huazhong University of Science and Technology. She is currently a full professor and Ph.D. supervisor at the National NC System Engineering Research Center at Huazhong University of Science and Technology. Her research has focused on machining surface integrity and multi-axis machining accuracy compensation.

Author contributions Mr. **ZHANG Hua** designed the study, complied the models, conducted the analysis, interpreted the results, and wrote the manuscript. Prof. **YAN Rong**, Prof. **TANG Xiaowei** and Dr. **SUN Hao** guided the research and designed the article structure. Mr. **ZHAO Shengqiang**, Ms. **SHAN Yunan** and Prof. **PENG Fangyu** contributed to data preparation and background of the study. All authors commented on the manuscript draft and approved the submission.

Competing interests The authors declare no competing interests.

(Production Editor: XU Chengting)

初始残余应力的检测方法及其在薄壁叶片加工变形分析中的应用研究

张 华[1], 赵晟强[1], 孙 豪[1], 彭芳瑜[1,2], 闫 蓉[1], 唐小卫[1], 单玉楠[1]

(1.华中科技大学机械科学与工程学院国家数控系统工程研究中心,武汉 430074,中国;
2.华中科技大学机械科学与工程学院数字化制造装备与技术国家重点实验室,武汉 430074,中国)

摘要:薄壁叶片是航空发动机的关键部件,在加工过程中极易发生剧烈的变形。已有的变形研究控制重点关注在减小切削力和加工残余应力(Machining-induced residual stress, MIRS)这两方面。本文利用材料热处理和锻造过程中产生的初始残余应力(Initial residual stress, IRS)来减轻薄壁零件受切削力与加工残余应力影响所产生的变形。由于初始残余应力测量困难且具有破坏性,本文提出了一种初始残余应力逆辨识方法来测量Ti6Al4V的初始残余应力。与传统的初始残余应力测量方法相比,逆辨识方法更符合应力分布和叶片变形的分布趋势。为了研究和解耦初始残余应力、加工残余应力和切削力之间对加工变形影响的相互作用,针对钛合金直纹叶片为对象进行实验验证,并建立了有限元预测模型。在分析切削力与加工残余应力对变形的影响后,可以得到切削力占变形程度的46.17%,平均值为26.36 μm,而加工残余应力占变形程度的53.83%,平均值为30.70 μm。耦合初始残余应力后使得整体的变形减小,受加工残余应力影响的最大挠度变形从35.32 μm降低到15.50 μm,该分析为利用初始残余应力减小薄壁叶片加工变形提供了新的方法。

关键词:薄壁叶片;加工变形;残余应力分析;切削力模型